Vol. 37, No. 4 (2015) 427-433

Tribology in Industry

www.tribology.fink.rs

RESEARCH

Experimental Determination of Contact Area

O. Maršálek[a], J. Dlugoš[a], P. Raffai[a], P. Novotný[a], J. Knotek[a]

[a]*Institute of Automotive Engineering, Brno University of Technology, Czech Republic.*

Keywords:

Contact pressure
Multibody System
Rough surface
Contact resistivity

Corresponding author:

Ondřej Maršálek
Institute of Automotive Engineering,
Brno University of Technology,
Czech Republic.
E-mail: marsalek@fme.vutbr.cz

A B S T R A C T

The main goal of this article is to experimentally evaluate the contact area and to compare the measured results with the different contact model theories. The experiment takes advantage of the electrical contact resistivity principle in a dry piston/cylinder liner test rig assembly. Analytical contact models are implemented into the computational simulation. The calculated contact area depends on the dynamics and precomputed database of contact pressure and contact area in the relation to the separation distance of surfaces. Multibody System (MBS) is augmented by a user-written FORTRAN subroutine and used for the solution.

1. INTRODUCTION

Monitoring of the contact area of two surfaces during dynamic simulation is a relatively complicated task, especially in the case of piston/cylinder liner interaction. With respect to the crawl-walk-run approach the following procedure was executed.

Authors of [1-4] describe the methodology for experimental estimation of the oil film thickness in a roller bearing. In all these sources the principle of electric current going through the lubricated contact pair is used. The thickness of oil film layer is then given by the electrical contact resistance. In this case the resistance becomes relatively high due to the oil insulating properties. When this principle is applied to a dry contact the electric current goes through a high number of micro-contacts which can be represented by collaterally connected resistors. Thus, the total value of electrical resistance is very low.

Reasons for this research are supported, for example, by statements mentioned in [5] where authors present that production of CO_2 emissions of internal combustion engines are derived also from the frictional losses of combustion engine parts.

Furthermore, the paper [6] presents how big portion of overall losses of combustion engine is created by mechanical losses and how big contribution to the process of decreasing of mechanical losses (leading to the lower fuel consumption and thus also lower CO_2 emissions) can have even a small modification of surface pattern geometry.

These information, among others, lead to the impression that the attention of similar

computational models should be paid to the development of more precise algorithms which can fully use the potential of contemporary hardware; and therefore, help with the development of more environmentally friendly combustion engines.

The aim of this paper is to apply the above mentioned experimental methodology on a dry contact, so the contact area can be estimated and compared with different analytical contact models.

This paper extends and refines information from the source [7] where the process of numerical solution of transition between pure hydrodynamic lubricating regime and mixed lubrication regime is described. In other words: how big influence the surface pattern of machinery parts has on the hydrodynamic lubricating layer.

2. ANALYTICAL CONTACT MODELS

In this chapter all the theoretical analytical models for the contact pressure calculation are going to be described gradually.

2.1 Contact Model Greenwood & Tripp

The first analytical model is Greenwood & Tripp [8]. It is a very effective and widely used model, as nowadays as in the past. Based on these characteristic was this computational model chosen from all the implemented contact models. In this model, parameter ($\eta_r\beta\sigma$) has an essential impact on the contact pressure values. This parameter represents the surface pattern information: η_r is the surface density of asperities [m^{-2}], β is the average radius of asperity curvature [m] and σ is the combined root mean square (RMS) roughness of both surfaces [m]. According to the original information source [8] this parameter should be in the range between 0.03 and 0.05. Therefore, it is important to examine the value of this parameter during processing of the surface pattern characteristics data. When there is a significant deviation from the presumed range this model will provide biased or incorrect results of contact pressure.

For the description of surface pattern of both surfaces, optical profilometer Contour GT-X from BRUKER was used (Figs. 1 and 2). Input variables for this contact model are listed in the Table 1.

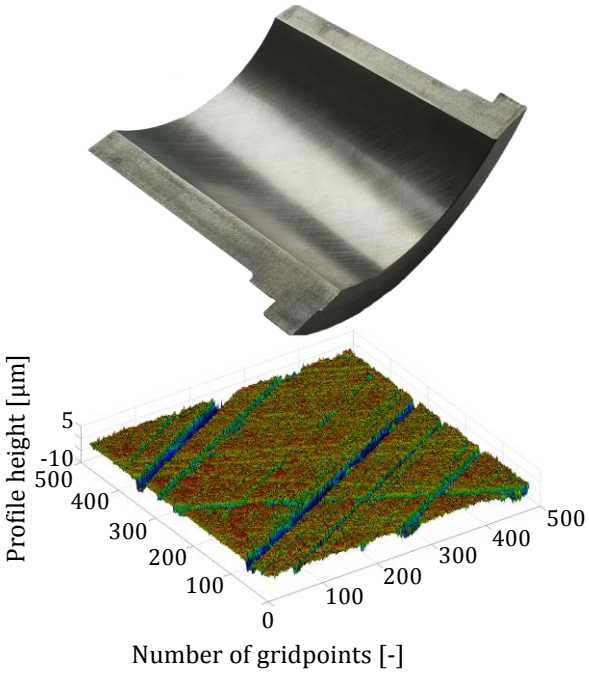

Fig. 1. Cut-out of the piston liner together with its surface pattern.

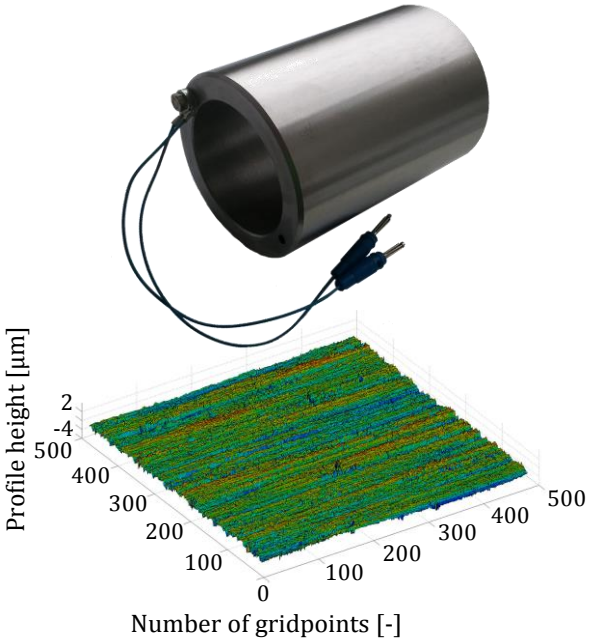

Fig. 2. Experimental piston with an example of its surface pattern.

The variable *Sds* has the same meaning here as variable η_r (density of asperities) used in the Greenwood & Tripp's theory. The variable *Ssc* can be very simply converted to the variable β (average asperity radius curvature) which corresponds to the terminology from the

Greenwood & Tripp's theory. The variable S_q (root mean square of each 3D surface profile) is directly used for calculation of the variable σ (combined root mean square of both surfaces) according the following formula:

$$\sigma = \sqrt{Sq_1^2 + Sq_2^2} \tag{1}$$

From the last column of the table can be seen that the parameter ($\eta_r\beta\sigma$) is close to the required range; and therefore, it is possible that the results of contact pressure given by this model will be biased. Therefore, it is necessary to consider these results only as informative.

Table 1. Measured data of rough surfaces.

Piston			Piston liner		
Sds [1/μm²]	*Ssc* [1/μm]	*Sq* [μm]	*Sds* [1/μm²]	*Ssc* [1/μm]	*Sq* [μm]
0.002601	0.123699	0.742373	0.003486	0.294883	1.245464
η_r [1/μm²]	β [μm]	*Sq* [μm]	η_r [1/μm²]	β [μm]	*Sq* [μm]
0.002601	8.084168	0.742373	0.003486	3.391175	1.245464
Average values					
η_r [1/μm²]	β [μm]	σ [μm]			
0.003043	5.737672	1.449930			
η_r [1/m²]	β [m]	σ [m]			
$3.043178\cdot10^{9}$	$5.737672\cdot10^{-6}$	$1.449930\cdot10^{-6}$			
($\eta_r\beta\sigma$)					
0.025317					

The basic equation for the contact pressure determination has a form:

$$p_c(h) = \frac{8\pi}{5}(\eta_r\beta\sigma)KF_{5/2}\left(\frac{h}{\sigma}\right) \tag{2}$$

Where:

$$K = \frac{2\sqrt{2}}{3}(\eta_r\beta\sigma)E'\sqrt{\left(\frac{\sigma}{\beta}\right)} \tag{3}$$

$$\frac{1}{E'} = \frac{1-\upsilon_1^2}{E_1} + \frac{1-\upsilon_2^2}{E_2} \tag{4}$$

Here ν is the Poisson's ratio [-], E' is the combined Young's modulus [Pa], $E_{1(2)}$ is the Young's modulus for each material of the contact pair [Pa] and $F_{5/2}$ is the function of contact pressure increase [-] (given by the table in the reference [8]).

2.2 Contact Model Hertz

For the comparison probably the most well-known contact model – Hertz [9] – was implemented. Input variables for this contact model are the deflection (penetration) of contacting bodies δ_R [m], the material characteristic Young's modulus E' [Pa] and the combined radius of curvature R' [m].

For contact models Hertz, Lagemann and Pasaribu & Schipper the identical way of combined radius of rough surfaces curvature calculation is used. This calculation is based on the osculation curve radius determination. This radius of curvature is determined for each point of surface rough profile in both directions (x and y). Radius of curvature of contact body 1 in the direction x is given by the equation:

$$R_{1x}(x) = \frac{\left(1+\left(z'(x)\right)^2\right)^{3/2}}{z''(x)} \tag{5}$$

As $z'(x)$ is here labelled as the first numerical derivation of the matrix with surface profile heights in the given point x. Then $z''(x)$ is the second numerical derivation of the matrix with surface profile heights in the given point x.

The rest of this computational model is given by the following formulae:

$$W = \sqrt{\frac{\delta_R^{\,3}E'^2R'}{1.0397^3}},\ a = \left(\frac{3WR'}{E'}\right)^{1/3} \tag{6}$$

$$P_{\max} = \frac{3W}{2\pi a^2},\ P_{av} = \frac{W}{\pi a^2} \tag{7}$$

Where W is the contact force [N], a is the radius of the contact area [m], and $P_{\max}$ and P_{av} determine the maximal and the average contact pressure [Pa].

2.3 Contact Model Lagemann

The next implemented contact model is the model published by Volker Lagemann in his dissertation thesis [10]. This model represents modified Hertz pressure formulae. Therefore, the results from this model are presumed similar to the results from the classical Hertz theory described in the previous chapter.

In comparison with the classical Hertz theory, here the formulae for calculation of the normally

acted contact force W [N], for calculation of radius of contact area a [m], and also formulae for maximal and average contact pressure P_{max} and P_{av} [Pa] are changed:

$$W = \sqrt{\frac{16\delta_R^{\ 3} E'^2 R'}{9}},\ a = \left(\frac{3WR'}{4E'}\right)^{1/3} \tag{8}$$

$$P_{\max} = \frac{1}{\pi}\sqrt{\frac{6E'^2 W}{R'^2}},\ P_{av} = P_{\max}\sqrt{1+\frac{\delta_R^{\ 2}}{a^2}} \tag{9}$$

Because of the need to maximally capture the physical essence of the problem besides the selected contact models involved was also a contact model taking into consideration all the possible states of material behaviour – fully elastic, elasto-plastic, and fully plastic.

2.4 Contact Model Pasaribu & Schipper

This contact model was published by authors Pasaribu & Schipper [11]. In comparison with all the above described contact models here is an additional input variable – the hardness of the softer material from the contact pair H [Pa].

Transitions between the individual material behaviours are controlled by the depth of the penetration. Boundary values of penetration (deflection) (ω_c [-]) are given by following equations:

$$\omega_{c1} = 0.89R'\left(\frac{H}{E'}\right),\ \omega_{c2} = 54\omega_{c1} \tag{10}$$

The contact behaves elastically if condition $\delta_R < \omega_{c1}$ is met. The elasto-plastic behaviour of the contact pair is considered in the case when condition $\omega_{c1} < \delta_R < \omega_{c2}$ is valid. And finally – the condition for fully plastic behaviour is given by the relation $\omega_{c2} < \delta_R$.

If materials behave plastically the calculation of the contact area A_{el} [m²] and contact force F_{el} [N] is given by the following equations:

$$A_{el} = \pi R'\delta_R,\ F_{el} = \frac{4}{3}E'R'^{0.5}\delta_R^{\ 1.5} \tag{11}$$

In the case of elasto-plastic behaviour of contact pair the calculation of contact area A_{ep} [m²] and contact force F_{ep} [N] uses the following formulae:

$$A_{ep} = \pi R'\delta_R\left[1-2\left(\frac{\delta_R-\omega_{c1}}{\omega_{c2}-\omega_{c1}}\right)^3+3\left(\frac{\delta_R-\omega_{c1}}{\omega_{c2}-\omega_{c1}}\right)^2\right] \tag{12}$$

$$F_{ep} = \left[H-0.6H\frac{\ln\omega_{c2}-\ln\delta_R}{\ln\omega_{c2}-\ln\omega_{c1}}\right]A_{ep} \tag{13}$$

The final scenario is when materials behave plastically. Then for the contact area A_p [m²] and contact force F_p [N] the following two equations are used:

$$A_p = 2\pi R'\delta_R,\ F_p = HA_p \tag{14}$$

The contact pressure for all three possible scenarios listed above is calculated according to the classic formula for pressure determination (pressure equals force divided by area).

3. MBS MODEL

To compare the experiment with one of the contact theories, the computational model needs to be created. While doing so, it is very important to keep in mind the Saint-Venant's principle, which says: *"The difference between the effects of two different, but statically equivalent loads becomes very small at sufficiently large distances from load."* According to this theory, contact issue between the piston and the cylinder liner can be seen differently.

From the macroscopic point of view, if the two round shaped contacting bodies are rigid, only a single force will act upon the single point of contact. In the different case of flexible bodies, the contact region will widen and cause the contact force to spread as it is shown in Figure 3. Moreover, the deformation is not only present in the region of the contact force applied. The deflection of one node affects its adjacent neighbours as well. The overall size of the contact area is evaluated as the total sum of elements active in the contact. This approach is greatly supported by the finite element method.

On the other hand, from the microscopic point of view, the contact forces of two rough surfaces are carried by its asperities (Fig. 3). As previously mentioned, considering the two contacting bodies rigid, while the asperities can deform locally. Contact forces result in a deformation of each active asperity. The number of asperities in contact, the contact pressure and the size of the overall contact area are, therefore, dependent on the nominal surface distance h. Global elastic (plastic) deformation of bodies affects this nominal surface distance.

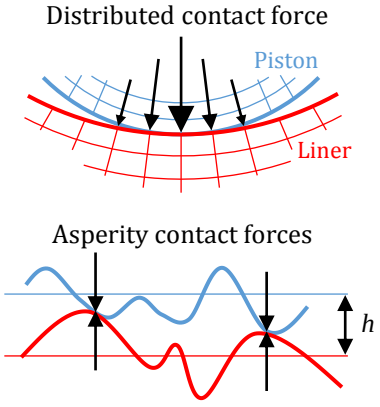

Fig. 3. Contact of two flat flexible bodies and rough surface contact.

From the computational algorithms presented in the previous chapter (Chapter 2) a database of contact pressures and contact areas, depending on the separation distance of analysed surfaces, was created for the MBS simulation. Trends of all contact curves are shown in Fig. 4. Because the values of contact pressure given by the Greenwood & Tripp model were too different (lower), this curve was plotted on the secondary axis of the graph. The reason is the deviation of the parameter ($\eta_r\beta\sigma$) which should be in a range between 0.03 and 0.05 [8]. If the tested surfaces are not within this range, we can expect biased results. In this case the measured parameter ($\eta_r\beta\sigma$) was 0.025. Volker Lagemann [10] also confirmed the lower contact pressure values of Greenwood & Tripp model.

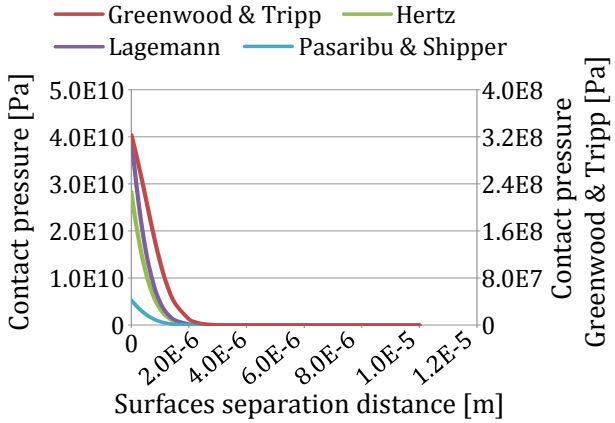

Fig. 4. Contact pressure dependence on surfaces separation.

Due to the application of low loads (Figure 9), the elastic deformations of each body contact region is considered negligible and plastic deformations are not expected at all. Therefore, the MBS model with rigid bodies is sufficient. Commercially available MSC ADAMS enhanced by FORTRAN user-written subroutine was used as MBS software. MBS-subroutine solution loop is shown in Fig. 5.

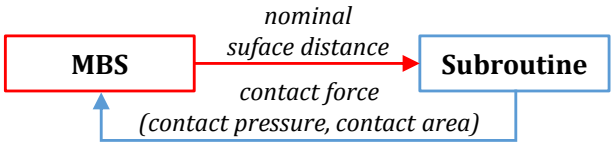

Fig. 5. Flowchart of piston/cylinder liner simulation.

In the MBS, the piston and the cylinder liner overlay by the computational nodes, where the contact forces take place. Each computational node represents a specific area – an element. Since the element is characterized by only one node, the nominal surface distance is considered constant across the whole element surface. This requires small element size at the contact regions to simulate the interaction properly. For such purpose, node density is adapted to the expected location of contact regions (Fig. 6). This approach provides acceptable speed of simulation with accurate results.

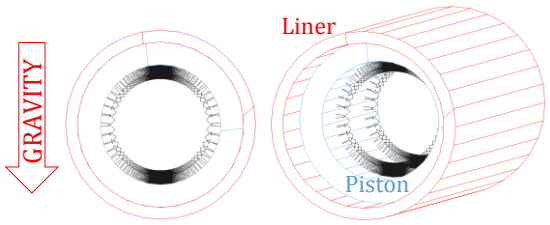

Fig. 6. Computation nodes refinement.

To suppress the unwanted fluttering of the piston, a damping force is introduced. The overall contact force then takes form:

$$F_{c\_MBS} = P_c A_c + B_{MBS} v_{MBS} \quad (14)$$

Where F_{c_MBS} is the contact force [N], P_c is the contact pressure [Pa], A_c is the contact area [m^2], B_{MBS} is damping [N·s·m^{-1}] and v_{MBS} is the relative speed of both surfaces [m·s^{-1}]. The computational model simulates a static equilibrium of the forces between the piston and the cylinder liner actuated by the gravity (no motion in the axis of the cylinder liner is applied).

4. RESISTIVITY PREDICTION

Following relations were used for the design of the measuring circuit [3]:

$$R_T = \frac{\zeta h_R}{A_R}, \; I = U_R / (R_T + R_{Piston} + R_{Liner}) \quad (15)$$

Where R_T is the resistivity of the contact [Ω], R_{Piston} is the resistivity of the piston [Ω], R_{Liner} is the resistivity of the cylinder liner [Ω], A_R is the contact area [m²], h_R is the height of electrical contact [m], ζ is the resistance of material [Ω·m] and I is the electric current [A].

The measuring circuit was initially designed according to the following Fig. 7.

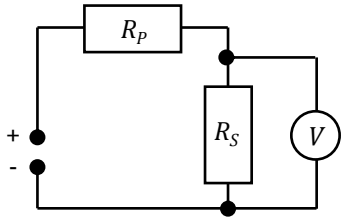

Fig. 7. Primarily designed electrical scheme: R_P – added resistance.

When the measuring circuit was finished, greater (than predicted) values of resistivity were measured. Therefore, it was possible to remove the additional resistor.

The experimental device was designed according to Fig. 8. Crankshaft motion was constrained so the experiment could be performed as the simplest scenario. The intentionally chosen design of the experimental piston allows the insertion of a weight inside the piston body. Thus, it is possible to gradually change the acting force between the piston and piston liner and to observe the contact area changes.

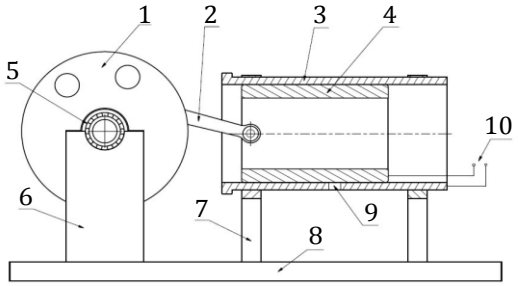

Fig. 8. Test rig scheme: 1 – crankshaft powered by electric engine, 2 – connecting rod, 3 – piston liner, 4 – experimental engine, 5 – crankshaft mount, 6 – crankshaft bearing housing, 7 – piston liner support, 8 – base, 9 – oil intake, 10 – cables for electric circuit connection.

5. RESULT DISCUSSION

5.1 Experiment

The measurement was done by device Keithley 6221/2182A Delta mode system with AC and DC current source and a nanovoltmeter.

Measured values are very different from the ones predicted by the contact models listed in chapter 2. The main causes are: differences in resistance of both materials; impact of wires resistance; impact of transition resistance of contacts and connectors; different resistance of surface layer (oxidation, contamination), etc.

5.2 Comparison

Since the measurement was done for different weight loads applied, measured and calculated contact area values can be compared with the values of nominal load 53 N (5.440 kg), therefore the dimensionless ratios are available as depicted in Fig. 10.

Test rig bore was 76 mm (Fig. 8), while the maximal load force applied was 255 N (25.966 kg). These values are insufficient to cause any plastic deformations. In addition, only very low elastic deformations are present. All the implemented models provide very similar results under these conditions – surface separation above 3 μm (Fig. 2). Therefore, the graph in Figs. 9 and 10 does not clearly state which of the observed contact models is the most accurate.

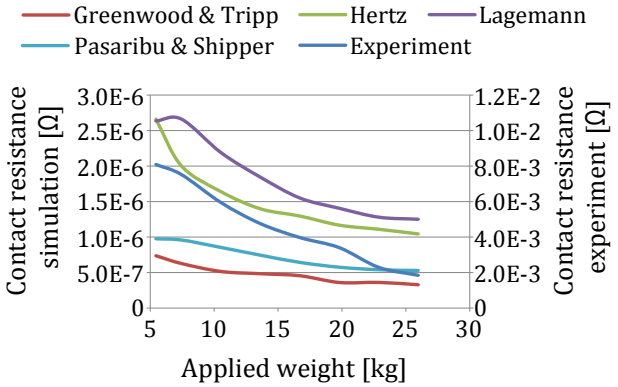

Fig. 9. Comparison of simulated and experimental results – absolute values.

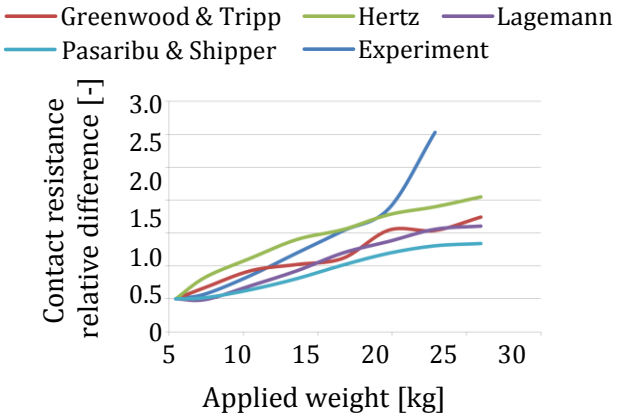

Fig. 10. Comparison of simulated and experimental results – relative values.

To highlight the differences between the contact models, large elasto-plastic deformations would have to be tested. Meaning that, the use of a hydraulic press would be necessary to create higher loads. MBS model would have to be modified as well – implementation of flexible bodies.

6. CONCLUSIONS

The designed test rig was, in this case, focused on the dry contact of piston/cylinder liner. The change in electrical contact resistance was able to record the differences in the contact area due to various loads applied, even when only very low elastic deformations were present – the measuring principle using contact resistance was proven.

Experimental and simulated data have similar trends, but the offset is significant. It is caused by the unknown resistance between the individual measuring circuit items. At this moment, the best from the selected analytical contact models cannot be determined. For this purpose, higher deformations would have to be introduced.

Further development of the test ring leading to the successful continuation of the experiment is suggested.

Acknowledgement

The research leading to these results has received funding from the Ministry of Education, Youth and Sports under the National Sustainability Programme I (Project LO1202).

REFERENCES

[1] H. Prashad, *Tribology in electrical environments.* Boston: Elsevier, 2006.

[2] Y. Jang and J. Barber, 'Effect of contact statistics on electrical contact resistance', *Journal of Applied Physics*, vol. 94, no. 11, 2003.

[3] S. Matharu, S. Sanyal and D. Bal, 'Development of a multipurpose, efficient and inexpensive bearing test rig', *Journal of Engineering and Technology Research*, no. 2, pp. 44-49, 2010.

[4] Z. Peng-shun, L. Shu-guang and Z. Wen-jie, 'A new measurement method of oil film thickness in the EHL condition: the R-C oscillation technique', *Wear*, vol. 148, no. 1, pp. 39-46, 1991.

[5] A. Sonthalia and C. Kumar, 'The Effect of Compression Ring Profile on the Friction Force in an Internal Combustion Engine' *Tribology in Industry*, vol. 35, no. 1, pp. 74-83, 2013.

[6] P. Mishra, 'A Review of Piston Compression Ring Tribology' *Tribology in Industry*, vol. 36, no. 3, pp. 269-280, 2014.

[7] O. Maršálek, P. Novotný and P. Raffai, 'Micro-lubrication of Directionally Oriented Contact Surfaces' *Tribology in Industry*, vol. 36, no. 4, pp. 451-464, 2014.

[8] J. Greenwood and J. Tripp, 'The contact of two nominally flat rough surfaces', in *Proceedings of the Institution of Mechanical Engineers 1847-1982 (vols 1-196)*, vol. 185, issue 1970, pp. 625-634, 1970.

[9] G. Stachowiak, *Engineering tribology. 4th ed*. Oxford: Butterworth-Heinemann, 2014.

[10] V. Lagemann, *Numerische Verfahren zur tribologischen Charakterisierung bearbeitungsbedingter rauher Oberflächen bei Mikrohydrodynamik und Mischreibung*. Dissertation. Kassel: Univ.-Bibliothek, 2000.

[11] H. Pasaribu and D. Schipper, 'Application of a Deterministic Contact Model to Analyze the Contact of a Rough Surface against a Flat Layered Surface', *Journal of Tribology*, vol. 127, issue 2, pp. 451-455, 2005.